Internalization and mechanisms of toxicity of lipid nanocapsules in HepG2 and HepaRG hepatoma cells upon acute and chronic exposures

Flavien Delaporte, Emilie Roger, Jérome Bejaud, Pascal Loyer, Frédéric Lagarce, Camille C Savary

International Journal of Pharmaceutics 667 (2024) 124815

Contents lists available at ScienceDirect

International Journal of Pharmaceutics

journal homepage: www.elsevier.com/locate/ijpharm

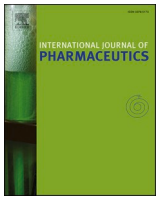

Internalization and mechanisms of toxicity of lipid nanocapsules in HepG2 and HepaRG hepatoma cells upon acute and chronic exposures

Flavien Delaporte [a,b,*], Emilie Roger [a], Jérome Bejaud [a], Pascal Loyer [c], Frédéric Lagarce [a,b], Camille C. Savary [a]

[a] Univ Angers, CHU Angers, Inserm, CNRS, MINT, SFR ICAT, F-49000 Angers, France
[b] CHU Angers, 4 rue Larrey, 49033 Angers, France
[c] Inserm, University of Rennes, INRAE, NuMeCan Institute (Nutrition, Metabolisms and Cancer), Rennes, France

ARTICLE INFO

Keywords:
LNCs
Toxicity
Liver
Repeated exposure
Internalization kinetics/pathways
Cytotoxicity

ABSTRACT

Lipid nanocapsules (LNCs) used as nanomedicine have been developed to enhance pharmacokinetics and decrease side effects of drugs, particularly for cancer therapies. After intravenous administration, LNCs possess an important hepatic tropism however, few data exist about their toxicity and even less after repeated exposure. This study aimed to assess the *in vitro* toxicity and internalization of unloaded LNCs, of 50 and 100 nm size, on HepG2 and HepaRG liver cell lines. Internalization of the 50 nm LNCs was slower compared to the 100 nm LNCs and both LNCs exhibited a higher toxicity on cancerous HepG2 cells compared to differentiated HepaRG cells. LNCs were mainly internalized via caveolin-mediated endocytosis in both cell lines. Upon chronic exposure, the toxicity of LNCs on HepaRG cells increased, although the pathways of internalization remained unchanged. Cell death studies have demonstrated an involvement of ferroptosis, but not of apoptosis. After acute and repeated exposures on HepaRG cells, the 100 nm LNCs showed a good safety profile. Finally, LNCs induced a more significant toxicity associated with faster internalization in the HepG2 cancerous model than in the differentiated HepaRG cells. This provides good evidence for LNCs to potentialize the cytotoxic effects of an active drug on liver cancer cells.

1. Introduction

At the end of the 20th century, nanoparticles (NPs) for medical applications (nanomedicines) appeared and the first nanomedicine was approved by the Food and Drug Administration (FDA) in 1995 (Barenholz, 2012). Over the past two decades, NPs have attracted great interest because of their capacity to improve the efficiency of drugs and reduce their side effects (Desai et al. 2012, Frank et al. 2015). The physicochemical properties of these nanocarriers, such as their size and composition, can be modified, which will result in changing their cellular interactions and by extension their safety (Fadeel et al. 2015, Ajdary et al. 2018). Different types of NPs can be used as therapeutics, such as liposomes, micelles, polymers and lipid NPs (Basile et al. 2012). Among lipid NPs, LNCs, which are spherical nanostructures composed of an oily core surrounded by a surfactant shell (Heurtault et al. 2002, Mouzouvi et al. 2017, Dabholkar et al. 2021), were selected for this study. LNCs demonstrate notably a real interest in treating cancers (Huynh et al. 2009). However, despite their potential advantages, LNCs, as well as any other nanoparticles, should be carefully characterized in terms of toxicity.

Several studies have already assessed the safety of LNCs on *in vivo* and *in vitro* systems. Single or repeated intravenous injections (IV) of unloaded LNCs induced no weight loss or histological or biochemical abnormalities in mice (Hureaux et al. 2010, Montigaud et al. 2018). Moreover, an *in vitro* study, interested in LNCs interactions with murine immune cells, showed that no genotoxicity occurred upon LNCs exposure (Le Roux et al. 2017). Nevertheless, regardless of the biocompatibility observed in the literature, LNCs hepatic toxicity has not been well characterized despite their well-demonstrated accumulation in the liver (Zhang et al. 2016, Resnier et al. 2019). This hepatic tropism can become an asset to treat diverse liver pathologies, such as hepatocellular carcinoma (HCC) (Schaffazick et al. 2008, Radwan et al. 2020). Generally, cancer treatment involves repeated medication for several months. Thus, it is necessary to evaluate the tolerance of LNCs in the liver after chronic exposure. Indeed, the liver is a crucial organ in the human body and plays a major role in drug metabolism. Besides, liver

* Corresponding author.
E-mail address: flavien.2606@gmail.com (F. Delaporte).

https://doi.org/10.1016/j.ijpharm.2024.124815
Received 3 April 2024; Received in revised form 6 October 2024; Accepted 7 October 2024
Available online 16 October 2024

toxicity remains a leading cause for the termination of further drug development in investigational programs and restrictions of use once the drug is in the market (Andrade et al. 2019). Therefore, rather the liver is or is not their main target, hepatic toxicity of LNCs must be characterized.

The use of *in vitro* liver-cell models is fast and convenient to study toxicity and responds to the new "3R" standards about animal ethics. HepG2 cells are a well-known cancerous model widely used and recommended by the U.S. FDA and the Nanotechnology Characterization Laboratory for nanotoxicity assessment (Protocols - Nanotechnology Characterization Lab - NCI, 2022). Nevertheless, this model expresses low metabolic activity and does not allow chronic studies. HepaRG cells, a differentiated liver cell model, express high metabolic activity (cytochromes, phase I and II enzymes) and are differentiated over one month. Moreover, the HepaRG cell line might be considered as no tumorigenic cells (Cerec et al. 2007). This model, currently the closest to the gold standard represented by primary human hepatocytes (Andersson et al. 2012, Mueller et al. 2014), will allow the evaluation of toxicity of LNCs after chronic exposure (Jossé et al. 2008, Anthérieu et al. 2010, Kammerer and Küpper 2018).

In this context, the main objective of this work was to study, *in vitro*, the interactions between 50 nm and 100 nm LNCs after exposure with cancerous HepG2 and differentiated HepaRG liver cell lines following acute and chronic exposures up to one month. The kinetics of internalization were studied as well as intracellular trafficking. Endocytic pathways were analyzed using two different inhibitors, namely chlorpromazine and genistein. In addition of classic viability assessment (mitochondrial and lysosomal activity, cell membrane integrity), an assessment of apoptosis and ferroptosis was performed to identify the type of cell death occurring upon LNCs exposure.

2. Materials and methods

2.1. Materials

Glacial acetic acid, staurosporine, dithiothreitol (DTT), 3-[dimethylammonio]-1-propanesulfonate, ethylenediaminetetraacetic acid (EDTA), piperazine-N,N′-bis(2-ethanesulfonic acid) (PIPES), Dulbecco's phosphate buffer saline (DPBS), trypsin (0.25 and 0.05 %), N-acetyl-asp-glu-val-asp-7-amido-4-methylcoumarin (Ac-DEVD-AMC), bovine serum albumin (BSA), non-essential amino-acids, sodium pyruvate, hydrocortisone, 3-(4,5-dimethylthiazol-2-biopyl)-2,5-diphenyltetrazolium bromide (MTT), 3-Amino-7-dimethylamino-2-methylphenazine (NRU), hydrochloridechlorpromazine hydrochloride (CPZ), genistein (GEN), dimethyl sulfoxide (DMSO), insulin from bovine pancreas, acetaminophen, penicillin/streptomycin and lactate dehydrogenase (LDH) cytotoxicity detection kit were obtained from Sigma-Aldrich (Munich, Germany; St. Quentin-Fallavier, France; Zwijndrecht, The Netherlands). Williams'E medium, minimum essential medium (MEM), HyClone® fetal bovine serum (FBS), BODIPY 581/591 C11, trypsin-EDTA (0.05 and 0.25 %) and GlutaMAX™ supplements were purchased from Fisher Scientific (Illkirch, France). Dutcher® FBS was purchased from Dutscher (Bernolsheim, France). Captex® 8000 was a gift from Abitec Corp. (Colombus, Ohio, USA). Lipoid® S100 and Kolliphor® HS15 were purchased from Lipoid GmbH (Ludwigshafen, Germany) and BASF (Ludwigshafen, Germany), respectively. Erastin and ferrostatin-1 were purchased from Selleck Chemicals (Houston, TX, USA). NaCl was purchased from Prolabo VWR International (Fontenay-sous-Bois, France). Ultrapure water was obtained using a Milli-Q® Advantage A10 System (Merck Millipore, Darmstadt, Germany).

2.2. Formulation and characterization of LNCs

2.2.1. Preparation of DiD-TPB

DiD-TPB was synthesized using a method previously described (Kilin et al. 2014, Roger et al. 2017). Briefly, 100 mg of 1,1′-dioctadecyl-3,3,3′,3′tetramethylindodicarbocyanine perchlorate (DiD, Life Technologies, Carlsbad, California, USA) was mixed with 0.71 g (20mol eq.) of sodium tetraphenylborate in ethyl acetate, which easily dissolved both the salts. Thin-layer chromatography confirmed the formation of the targeted salt, and the product progressed faster than the starting DiD perchlorate (dichloromethane/methanol, 95/5). After solvent evaporation, the product (DiD-TPB) was purified using column chromatography (dichloromethane/methanol, 95/5).

2.2.2. Formulation of LNCs

Unloaded-LNCs were formulated according to a solvent-free method using temperature phase inversion (Heurtault et al. 2002). The compositions are listed in Table 1. Briefly, Captex® 8000 and Lipoid® S100 were mixed under magnetic stirring at 60 °C. After cooling, Kolliphor® HS15, NaCl, and water were added. Three cycles of heating and cooling between 60 and 95 °C were performed under magnetic stirring. During the last cycle, water at 4 °C was added to obtain LNCs suspension. Magnetic stirring was maintained for 5 min (min) at room temperature. Finally, the unloaded-LNCs suspensions were filtered through 0.22 µm sterile polyethersulfone membrane (Dutscher, Bernolsheim, France).

To prepare DiD-loaded-LNCs, DiD-TPB was first solubilized at 2 % w/w in Captex® 8000.

2.2.3. Physico-chemical characterizations of LNCs

Concentration of LNCs is expressed in mg/mL and was calculated by dividing the weight of all excipients over the total amount of water. The size distribution, polydispersity index (PDI), and zeta potential were determined by dynamic light scattering and laser doppler electrophoresis using a Zetasizer® Nano Series DTS 1060 (Malvern Instruments S.A., Worcestershire, UK), respectively. LNCs were diluted to 1/400 in water. The size of the formulations was also determined using nanoparticle tracking analysis on a NanoSight NS300 device (Malvern Instruments S.A., Worcestershire, UK) with prior 1/350,000 and 1/500,000 dilutions in water applied to the 50 nm LNCs (50-LNCs) and 100 nm (100-LNCs) suspensions, respectively. The fluorescence of the DiD-LNCs was measured using a FluoroMax®-4 spectrophotometer (HORIBA Jobin Yvon Inc., New Jersey, USA). Fluorescence emission spectra were recorded at room temperature with 650 nm excitation wavelength, with an excitation slit width of 3 nm and an integration time of 0.5 s. Emission spectra were collected from 655 to 750 nm with a slit width of 2 nm and a 1 nm increment. The maximum intensity of DiD was recorded at 675 ± 1 nm.

2.3. Cells and cell culture conditions

2.3.1. HepG2 cell line

HepG2 cells (ATCC® HB-8065) were cultured from 3rd to 18th passages in MEM supplemented with 10 % (v/v) FBS, 1X non-essential amino acids, 1 mM of sodium pyruvate in solution, and antibiotic solution (100 units/mL penicillin, 100 µg/mL streptomycin) in a humidified atmosphere of 5 % CO2, 95 % air at 37 °C. Once the cells reached 80

Table 1
Composition of unloaded- and DiD-LNCs.

Constituents	50-LNCs	100-LNCs	50-DiD-LNCs	100-DiD-LNCs
	Amount in mg			
Lipoïd® S100	67.2	67.2	8.4	8.4
Captex® 8000	1000	1550	62.5	96.9
DiD-TPB (2 %) in Captex® 8000			62.5	96.9
Kolliphor® HS15	1050	850	131.3	106.3
NaCl	73.3	73.3	9.2	9.2
Purified water	1950	1600	243.7	200
Purified water at 4 °C	2500	3400	625	625

% confluence, they were washed with DPBS, trypsinized (trypsin-EDTA 0.25 %), and seeded at 2.10^4 cells/cm^2 in a 25 cm^2 flask.

2.3.2. HepaRG cell line

HepaRG cells (obtained from Biopredict International) were seeded at $2.6.10^4$ cells/cm^2 in a 75 cm^2 flask and cultivated from 12th to 18th passages in Williams'E medium supplemented with 10 % (v/v) FBS, antibiotic solution (100 units/mL penicillin, 100 µg/mL streptomycin), 1X GlutaMAX™, hydrocortisone (25 µg/mL), and insulin (5 µg/mL) in a humidified atmosphere of 5 % CO2, 95 % air at 37 °C. After two weeks of growth, once 100 % confluency was reached, 2 % DMSO was added to the media for 2 more weeks to potentiate differentiation in hepatocytes (50 %) and biliary cells (50 %). Then the cells were trypsinized (trypsin-EDTA 0.05 %) and seeded in multiwell (MW) plates of different format depending on the assay (details in the following sections).

2.4. Treatment with LNCs

2.4.1. Acute treatment

HepG2 and HepaRG cells were seeded in either 12, 24, or 96 MW plates according to the corresponding assay, and then treated only once with unloaded-LNCs before the viability assay, kinetics, and pathways of internalization assessment. The exposure times and unloaded-LNCs concentrations are detailed in the following sections.

2.4.2. Chronic treatment

Briefly, HepaRG cells were seeded after differentiation in either 12, 24, or 96 MW plates according to the corresponding assay and then exposed to unloaded-LNCs every 2 to 3 days while the media was renewed. After 2 and 4 weeks of treatment, viability, kinetics, and internalization pathways were evaluated. Endpoints of treatment and LNCs concentrations are detailed in the following sections.

2.5. Toxicity assessment

2.5.1. Cell viability measurement

MTT and NRU viability assays were used to evaluate the toxicity of the LNCs. HepG2 and HepaRG cells were seeded in 96 MW. Cells were treated for 24 h with LNCs concentrations ranging from 0.001 to 10 mg/mL and diluted in media supplemented with 10 % or 0 % FBS. The media was then removed, and 100 µL MTT solution (5 mg/mL diluted 10 times in non-supplemented medium) was added to each well for 1 h. MTT was subsequently removed, and 100 µL of DMSO was used to solubilize the MTT crystals. The plates were thoroughly mixed for 5 min before reading the absorbance at 540 nm using a Clariostar® plate reader (BMG Labtech, Champigny-sur-Marne, France).

2.5.2. Lactate dehydrogenase (LDH) release

Both hepatoma cell lines were seeded in 96 MW and exposed to LNCs concentrations, ranging from 1 to 10 mg/mL for 24 h. After centrifugation for 10 min at 250 × g, the supernatants were removed, diluted to 1/10 in media and mixed with the reagent (catalyst and dye from the kit) at a 1/1 ratio. After approximately 30 min of incubation at room temperature, the absorbance was measured at 490 nm using a Clariostar® plate reader.

2.6. Lncs uptake by liver cell lines

2.6.1. Kinetics of internalization

The uptake of DiD-LNCs by hepatoma cells was quantified by measuring DiD fluorescence using fluorescence-activated cell sorting (FACS). Briefly, HepaRG cells were seeded in a 24 MW plate and HepG2 cells in a 12 MW plate as previously described. Both cell lines were exposed to subtoxic LNCs concentrations (0.1, 0.25 and 0.50 mg/mL) diluted in supplemented media with 10 % or 0 % FBS, from 15 min to 24 h and from 4 h to 96 h for HepG2 and HepaRG cells, respectively. For HepaRG cells, fresh media (half of the total volume of treatment) was added at 48 h to maintain an optimal pH. The cells were then trypsinized from the plates and washed twice with cold PBS before measuring the fluorescence on a CytoFLEX LX. Samples were kept on ice at all times during washing steps. A total of 10,000 cells were gated and analyzed for each condition.

Regarding the chronic treatment conditions, HepaRG cells were exposed every 2 to 3 days to 0.25 mg/mL of unloaded-LNCs for either 2 or 4 weeks. Once this period was completed, the cells were treated with DiD-LNCs at the same concentrations for 4, 24, and 48 h. A total of 10,000 cells were gated and analyzed for each condition.

2.6.2. Pathways of internalization

The cell lines were exposed to the DiD-LNCs in the presence or absence of endocytosis-blocking agents. Clathrin-mediated endocytosis was inhibited by treatment with 20 µM chlorpromazine (Roger et al. 2009). In contrast, 200 µM genistein inhibited caveolin-mediated endocytosis (Rennick et al. 2021). Prior to LNCs exposure (0.25 mg/mL), cells were sensitized for 1 h with inhibitors. Then, HepG2 cells were treated with LNCs and inhibitors for 2 h and HepaRG cells for 4 h under two distinct conditions: at 4 and 37 °C. Due to the high capacity of chlorpromazine and genistein to bind proteins, all inhibitors and DiD-LNCs suspensions were prepared in FBS-free media (Marshak et al. 1985, Bian et al. 2004). The cells were then trypsinized, washed twice with PBS and kept on ice before analaysis.

For chronic treatment, HepaRG cells were repeatedly exposed to 0.25 mg/mL of unloaded-LNCs, followed by a 4 h exposure to DiD-LNCs. A total of 10,000 cells were gated and analyzed for each condition and for both acute and chronic treatment.

2.6.3. Confocal microscopy

HepG2 cells were seeded on a black 96 MW plate, with flat and clear bottom (obtained from Ibidi, Munich, Germany), to perform live cell imaging. This experiment was also performed on HepaRG cells but the images were not exploitable (data not shown). HepG2 cells were stained with 100 nM of LysoTracker® Green DND-26 (LysoTracker) to identify lysosomes. Cells were subsequently exposed to DiD-LNCs, and acquisitions were performed from the first seconds of exposure up to 2 h.

Images were obtained using a Leica TCS SP8 AOBS (Leica Microsystems, Wetzlar, Germany) equipped with a water immersion objective, HC PL APO CS2 40X/ON 1.10. Acquisitions were performed in 8 bits with a 1024 × 1024 pixel format and scanning speed of 400 Hz. Excitation of LysoTracker and DiD were realized with a 488 nm laser line from an argon laser (40 mW) and with a 633 nm gas laser He-Ne (10 mW), respectively. Fluorescence was then recovered using a hybrid detector (GaAsP) from 492 to 549 nm for LysoTracker, and from 635 to 727 nm for DiD. Optic sections of 1 µm thickness were collected using Super Z Galvo Stage Type H.

2.7. Investigation of death mechanisms

2.7.1. Apoptosis activity measurement

Both HepG2 and HepaRG cells were seeded in 12 MW plates. Cells were exposed for 4 and 24 h to LNCs at 1 and 2 mg/mL, and 5 µM staurosporine was used as positive control. The caspase-3 activity was chosen to analyze apoptosis induced by LNCs exposure, using Ac-DEVD-AMC as a probe. After LNCs exposure, the supernatants were collected, and the cells were scraped with cold PBS. Supernatants and cells were mixed and centrifuged at 5000xg for 5 min at 4 °C. Supernatants were discarded, cells were resuspended in caspase activity buffer (20 mM PIPES pH 7.2, 100 mM NaCl, 1 mM EDTA, 0.1 % 3-[dimethylammonio]-1-propanesulfonate used to normalize the samples in terms of protein quantity. Finally, 30 µg of protein was incubated with 80 µM Ac-DEVD-AMC for 1 h at 37 °C in caspase-activity buffer containing 10 mM of DTT was added. The AMC part of the probe is cleaved by active caspases present in the apoptotic cell lysate and can be measured using a

fluorimeter because of its emission at 440–460 nm. The results were read on a Clariostar® plate reader at an excitation/emission wavelength of 380/440 nm.

2.7.2. Ferroptosis measurement

HepG2 and HepaRG cells were seeded in 96 MW plates as previously described. Both hepatoma cell lines were exposed for 24 h to LNCs concentrations ranging from 0.5 to 5 mg/mL, with or without the addition of ferrostatin-1 (FER) at 1 μM. Subsequently, the MTT assay was performed and the absorbance was red at 540 nm using a Clariostar® plate reader.

2.7.3. Lipid peroxidation activity

HepaRG and HepG2 cells were seeded in 12 MW plate as previously described. Concentrations of LNCs were ranging from 0.5 to 2 mg/mL and 1 to 5 mg/mL for HepG2 and HepaRG, respectively. After exposure, the cells were two times with tempered PBS, followed by 30 min of staining with the BODIPY™ 581/591 C11 (Bodipy-C11) probe at 5 μM. The cells were rinsed three times with tempered PBS, subsequently trypsinized and rinsed again twice before analysis. The fluorescence of the probe shifted from 590 nm (reduced state) to 510 nm (oxidized state). The results were read using the B525-FITC channel (525/40 nm) on a CytoFLEX LX (Beckman Coulter, Brea, CA, USA), and 10,000 cells were gated for each condition.

2.8. Data analysis

The results are expressed as mean values of one experiment in triplicate ± standard error of the mean (SEM) from at least 3 independent experiments. Mann-Whitney and Kruskal-Wallis tests were used for statistical and comparative analyses between two groups and three or more groups, respectively. In both cases, statistical significance was set at $p < 0.05$.

3. Results

3.1. Characterization of LNCs

LNCs of two different sizes were obtained. The mean hydrodynamic particle diameters in intensity were close to 50 and 100 nm for both unloaded-LNCs and DiD-LNCs, as shown by the DLS and NTA measurements (Table 2). A polydispersity index (PDI) lower than 0.200, a neutral ζ-potential for DiD-LNCs and unloaded-LNCs were obtained. For DiD-LNCs a close fluorescence intensity was obtained between the two sizes (Table 2).

Table 2
Characterization of unloaded- and DiD-LNCs: mean particle size in intensity (Zetasizer®) and in number (Nanosight NS300), polydispersity index (PDI), zeta (ζ)-potential and fluorescence intensity. Data are shown as mean ± SEM.

Type of LNC	Mean particle size (nm)		PDI	ζ-potential (mV)	Fluorescence intensity
	Zetasizer®	NanoSight NS300			
50-LNCs (n = 16)	52.2 ± 3.6	48.7 ± 2.5	0.057 ± 0.029	−2.4 ± 1.6	
100-LNCs (n = 16)	106.4 ± 6.2	98.6 ± 5.5	0.075 ± 0.016	−2.8 ± 2.7	
50-DiD-LNCs (n = 14)	57.9 ± 3.6	51.7 ± 5.5	0.127 ± 0.073	−2.4 ± 6.0	338 458 ± 37 566
100-DiD-LNCs (n = 12)	104.0 ± 7.2	91.8 ± 5.8	0.078 ± 0.031	−7.9 ± 4.9	447 158 ± 89 626

3.2. Toxicity assessment

3.2.1. Cell viability after acute and chronic exposure

LNCs toxicity profiles were evaluated by measuring mitochondrial activity using the MTT assay after 24 h of exposure to 0 or 10 % FBS and varying concentrations from 0.001 to 10 mg/mL (Fig. 1). The same toxicity was found with unloaded-LNCs and DiD-LNCs (data not shown). Both LNCs sizes induced a dose-dependent decrease in HepG2 and HepaRG cell viability. The 50-LNCs induced a significant decrease in cell viability by 50 % at 1 mg/mL in the HepG2 cell line compared to the 100-LNCs, which decreased cell viability by 25 % at the same concentration in the presence of FBS. The toxicity of 50-LNCs was significantly higher ($p < 0.05$) than 100-LNCs in HepG2 and HepaRG cells; LC_{50} values decreased from 1.57 ± 0.12 mg/mL to 0.94 ± 0.19 mg/mL and from 9.01 ± 0.41 mg/mL to 7.43 ± 0.65 mg/mL, respectively (Table 3). Lysosomal activity was also assessed (Supplementary data, Figure S1) and the results were similar to those of the MTT assay.

Cell viability was also assessed in HepaRG cells after 2 and 4 weeks of repeated exposure to varying concentrations ranging from 0.001 to 5 mg/mL (Fig. 1 and Supplementary Data, Figure S1). The corresponding LC_{50} calculated from the curves highlighted a time-dependent toxicity of 50-LNCs. For 100-LNCs the toxicity was higher after 2 weeks of exposure compared to 24 h but not higher after 4 weeks compared to 2 weeks. After 2 weeks of treatment, no difference between sizes was found. After 4 weeks of treatment, influence of size on toxicity was observed with 50-LNCs inducing more toxicity on HepaRG cells ($p < 0.05$) (Table 3).

3.2.2. LDH activity

Loss of membrane integrity was assessed by measuring the release of LDH into the supernatant after 24 h of exposure to the LNCs (Fig. 2). LNCs treatments of HepG2 cells induced an approximately 6 to 12-folds release of LDH compared to basal levels in negative control cultures. No significant differences were observed between the 50- and 100-LNCs (Fig. 2. A). 50-LNCs triggered LDH release in HepaRG cells in a concentration-dependent manner, from 7-to 15-fold at concentrations of 1 to 10 mg/mL. 100-LNCs significantly increased the release of LDH from 2 mg/mL (Fig. 2. B).

3.3. Lncs uptake by hepatoma cell lines

3.3.1. Kinetics of LNCs internalization after acute and chronic exposure

Three non-toxic concentrations of LNCs (0.10, 0.25 and 0.50 mg/mL) were used for assessment of uptake kinetics by cells. Only the results obtained with the intermediate 0.25 mg/mL concentration are presented because no difference on the uptake was observed between the 3 concentrations (data not shown).

The kinetics of LNCs internalization were determined by flow cytometry through the determination of two parameters: the percentage of positive cells and the mean fluorescence, reflecting the intracellular accumulation of LNCs (Fig. 3). For 50-LNCs, 35 % of cells were positive compared to 85 % for 100-LNCs in HepG2 cells after 1 h of treatment (Fig. 3. A), whereas in HepaRG cells, approximately 30 % positive cells and less than 50 % positive cells were observed for the 50-LNCs and 100-LNCs, respectively, after 4 h of exposure (Fig. 3. B). Hence, the internalization of 100-LNCs was faster in both the cell lines. Additionally, a difference between HepG2 and HepaRG cells was observed: 90 % internalization in HepG2 cells was achieved at 1 h *vs.* 24 h in HepaRG for 100-LNCs and at 2 h *vs.* 48 h for 50-LNCs.

Fig. 3. D and E represent the LNCs kinetics results expressed as median fluorescence intensity (MFI), which provided an estimation of LNCs intracellular accumulation. After 2 h of exposure, LNCs continued to accumulate in HepG2 cells for up to 24 h (Fig. 3. D). In the HepaRG cell line, exposure was extended up to 96 h, and an increase in intracellular

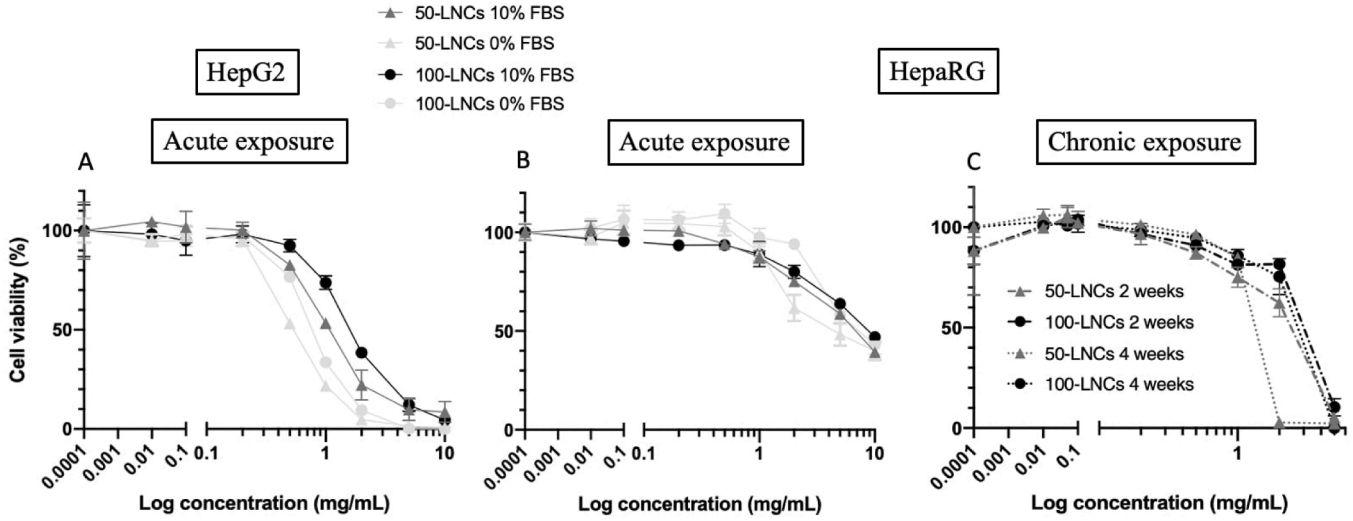

Fig. 1. Cell viability assessed by MTT assay on HepG2 cells (A) and HepaRG cells (B and C). The acute exposure was assessed in 10 % FBS and FBS-free condition (A and B) after 24 h of exposure. The chronic 2- and 4-weeks exposure (C) was assessed only on HepaRG in 10 % FBS conditions. Data are presented as % of viability in vehicle control cells (n = 4) ± SEM. Mitochondrial activity measurement allowed the determination of LC_{50} and non-toxic working concentrations. Classic 24 h exposure was performed as well as, for the first time, the cytotoxicity induced by LNCs after 2 and 4 weeks of exposure. Regarding *in vitro* results, a percentage of viability higher than 70 % confirms a low toxicity.

Table 3
Lethal concentration at 50 % of cell viability (LC_{50}), of 50- and 100-LNCs after 24 h of exposure on HepG2 and HepaRG cells, with 0 or 10 % of FBS, and after 2 and 4 weeks of exposure on HepaRG cell line. Data are shown as LC_{50} (mg/mL) (n = 3–5) ± SEM. X, *, # and + represents a significative difference between FBS effect, LNCs size, cell lines and times of exposure (2 weeks *vs.* 1 day and 4 weeks *vs.* 2 weeks), respectively ($p < 0.05$).

		Time of exposure (days)			
		1		14	28
		10 % FBS	0 % FBS		
HepG2 cells	50-LNCs	0.94 ± 0.19 *#	0.54 ± 0.04 x*#		
	100-LNCs	1.57 ± 0.12 *#	0.73 ± 0.10 x*#		
HepaRG cells	50-LNCs	7.43 ± 0.65 *#+	3.16 ± 1.98 x*#	2.25 ± 0.73 +	1.18 ± 0.08 *+
	100-LNCs	9.01 ± 0.41 *#+	7.16 ± 2.33*#	3.00 ± 0.24 +	2.57 ± 0.49 *

fluorescence was also observed. Within the first 48 h of exposure in the HepaRG model, a size effect was also detected with the highest 4-fold difference at 24 h; MFI values were approximately 1,000 and 4,000 for 50-LNCs and 100-LNCs, respectively. Thus, 100-LNCs accumulated more than 50-LNCs in both the cell lines. Finally, MFI was higher in HepG2 cells than in HepaRG cells after 24 h; approximately 10-fold and 4-fold higher for 50-LNCs and 100-LNCs, respectively.

After chronic treatment, the 100-LNCs remained internalized faster than the 50-LNCs after 4 h and 24 h of exposure (Fig. 3. C). Moreover, the 100-LNCs accumulated more intracellularly (Fig. 3. F).

In addition, internalization was investigated using confocal microscopy. In this experiment, LysoTracker was used to stain lysosomes and observe whether the LNCs colocalized with them upon internalization (Fig. 4). LNCs barely entered the HepG2 cells after 1 h (data not shown). Nevertheless, after 2 h, DiD-red fluorescence was detectable inside the cytosol for both LNCs sizes. Furthermore, some orange dots were observed corresponding in some colocalization of LNCs with lysosomes.

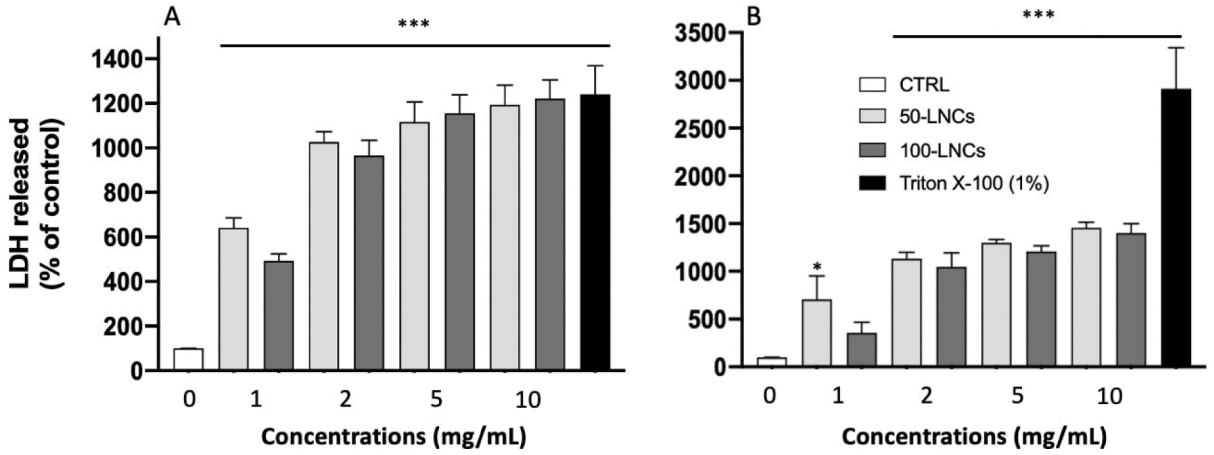

Fig. 2. Assessment of LDH release after 24 h of exposure to 50- and 100-LNCs on HepG2 (A) and HepaRG (B) cells. Data are shown as % of LDH released compared to control (n = 3–4) ± SEM. *($p < 0.05$) and ***($p < 0.001$) represent a significative difference compared with vehicle control. Negative (white histogram) and positive control (black histogram) are represented by cells non-exposed to LNCs and treated with Triton X-100, respectively. Absorbance has been measured with orbital detection in order to avoid any edge or center effect which can induce biases during measurement.

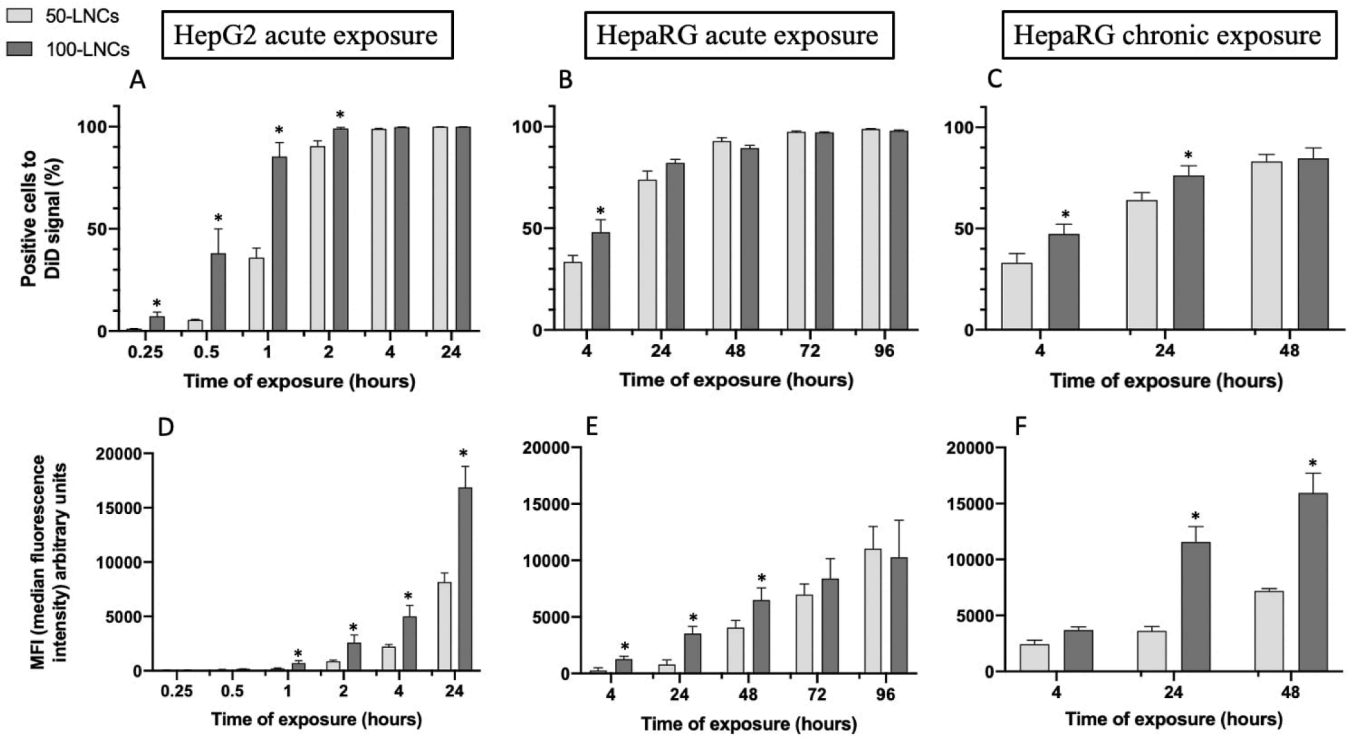

Fig. 3. Internalization of 50- and 100-LNCs in HepG2 (A and D) and HepaRG (B and E) cell lines after acute exposure, and in HepaRG cells after chronic exposure (C and F). Data represent % of positive cells to DiD signal (A, B and C) and median fluorescence intensity (MFI) in arbitrary units (D, E and F) (n = 3–4) ± SEM. *($p < 0.05$) represents a significative difference between sizes.

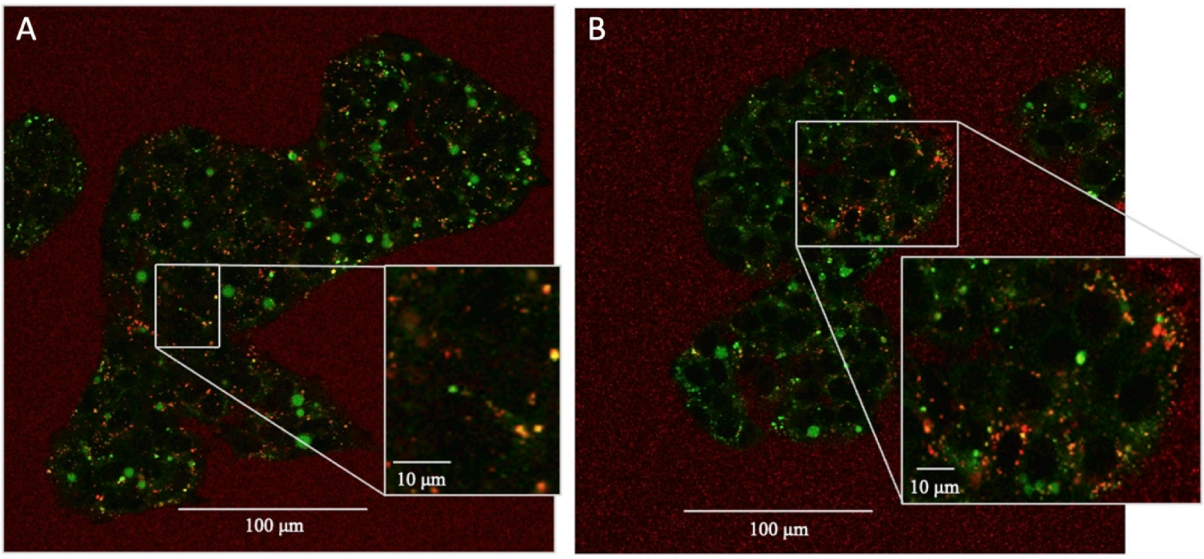

Fig. 4. Evaluation of the internalization of 50- (A) and 100-LNCs (B) in HepG2 cells by live imaging confocal microscopy after 2 h of exposure. DiD loaded-LNCs were used (red) and lysosomes were stained with LysoTracker (green). Colocalization of LNCs with lysosomes appears in orange/yellow.

3.3.2. Pathways of internalization after acute and chronic exposure

LNCs mechanism of internalization was explored using two different endocytosis blocking agents and at 4 and 37 °C. Previously, the viability of HepG2 and HepaRG cells was assessed by the MTT assay in the presence of inhibitors alone or in association with LNCs, and no toxicity was detected (Supplementary data, Figure S2).

At 4 °C, approximately 80 % of internalization for both LNCs was inhibited in HepG2 cells (Fig. 5. A and D). In HepaRG, approximately 60 % of internalization was blocked at 4 °C for both LNCs sizes (Fig. 5. B and E). In HepG2 cells, chlorpromazine had no effect on internalization, whereas genistein led to 50 and 40 % internalization inhibition for 50- and 100-LNCs, respectively. Similar results were obtained on the HepaRG cells. After repeated exposure for 4 weeks, comparable results to acute exposure were obtained for internalization study in the presence of chlorpromazine and genistein inhibitors (Fig. 5. C and F).

3.4. Investigation of death mechanisms

3.4.1. Apoptosis activity

The apoptosis was studied using the Ac-DEVD-AMC assay. This

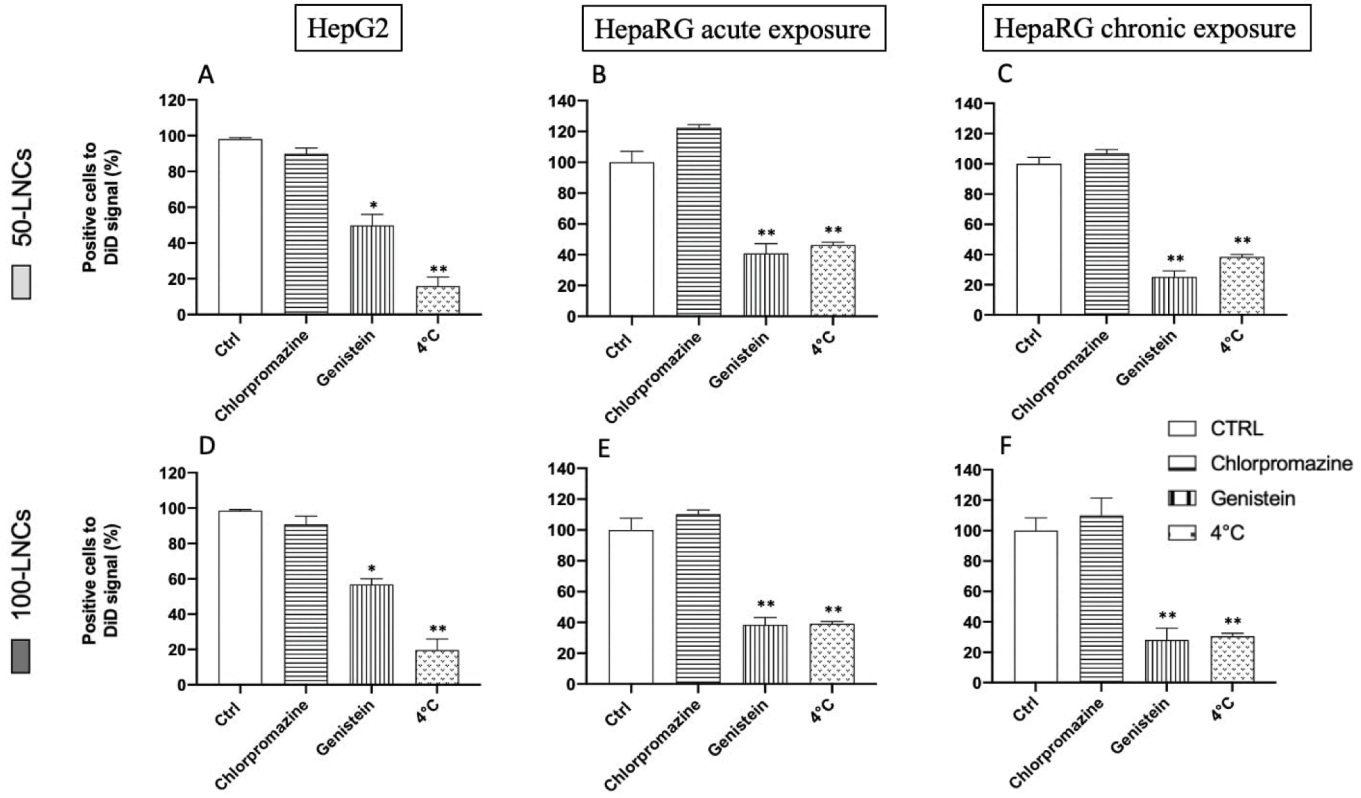

Fig. 5. Assessment of endocytosis-mediated pathways of internalization of 50-LNCs (A, B and C) and 100-LNCs (D, E and F) after acute exposure on HepG2 cells (A and D) and HepaRG cells (B and E), and after chronic exposure on HepaRG cells (C and F). Data are expressed in % of positive cells to DiD signal (n = 3) ± SEM. *($p < 0.05$) and **($p < 0.001$) represent a significative difference compared to the control. Chlorpromazine and genistein were used to inhibit CME and CavME, respectively. The 4 °C condition allowed to inhibit energy dependent transport systems.

fluorescent probe was used to measure caspase-3 activity after 4 and 24 h of exposure to 1 and 2 mg/mL of LNCs suspension (Fig. 6). The levels of caspase-3 activity for each LNC at every concentration did not differ from those observed under control conditions in both cell lines. No apoptosis activation via the caspase-3 pathway was observed in cells incubated with unloaded-LNCs, in contrast to the increased activities detected in the staurosporine positive control condition.

3.4.2. *Ferroptosis*

To evaluate whether ferroptosis is involved in cell death mechanisms, hepatoma cell lines were exposed to LNCs in the presence or absence of a specific ferroptosis inhibitor, FER (Fig. 7). Mitochondrial metabolic activity was measured after exposing cells to LNCs for 24 h with or without FER. The use of FER significantly maintained a higher metabolic activity (by ~25 %) in cells incubated with 50-LNCs at concentrations from 0.5 to 2 mg/mL in HepG2 cells while no difference was observed for 100-LNCs (Fig. 7. A). In HepaRG cells, FER increased metabolic activity by 10 % for both LNCs formulations and at every concentration, except at 1 mg/mL (Fig. 7. B).

3.4.3. *Lipid peroxidation*

The ability of LNCs to trigger lipid peroxidation was assessed using a Bodipy-C11 fluorescent probe (Fig. 8). A slight increase in lipid peroxidation was observed after 4 h of exposure to both LNCs sizes on HepG2 cells (Fig. 8. A). More importantly, lipid peroxidation was induced by LNCs after 24 h of exposure in a non-concentration-dependent manner.

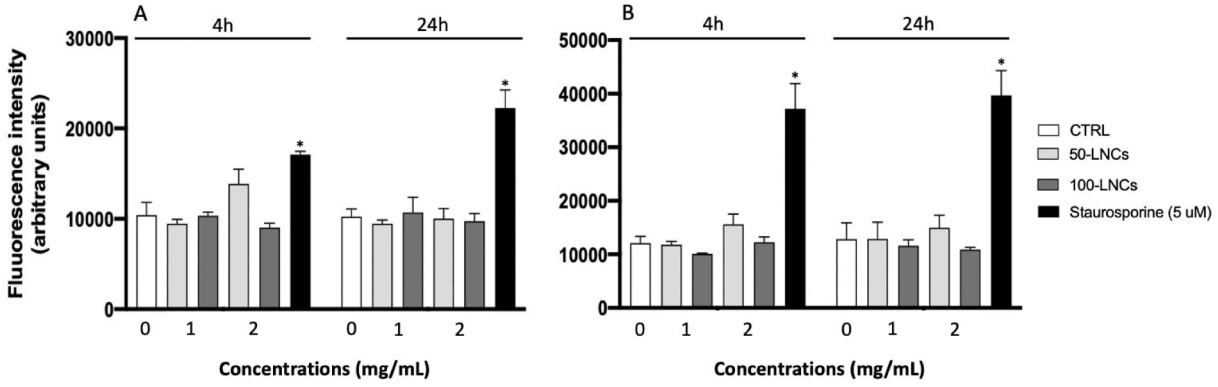

Fig. 6. Caspase-3 activity quantified by Ac-DEVD-AMC assay on HepG2 (A) and HepaRG (B) cells after 4 and 24 h of exposure to 50- and 100-LNCs. Data are shown as fluorescence intensity (n = 3) ± SEM. *($p < 0.05$) represents a significative difference compared to the respective control group. Caspase-3 activity reflects a cell death mechanism involving apoptosis.

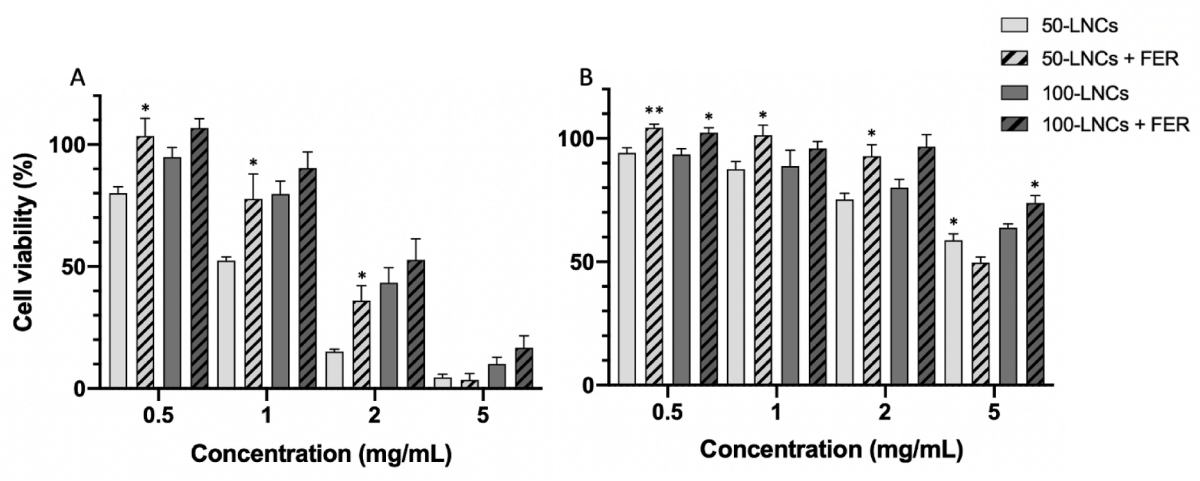

Fig. 7. Ferroptosis assessed by measuring cell viability (MTT), with or without ferroptosis inhibitor (FER), on HepG2 (A) and HepaRG (B) cells after 24 h of exposure to 50- and 100-LNCs. Data are presented as % of viability (n = 3–5) ± SEM. *($p < 0.05$) and **($p < 0.01$) represent a significative difference between samples treated or not with FER.

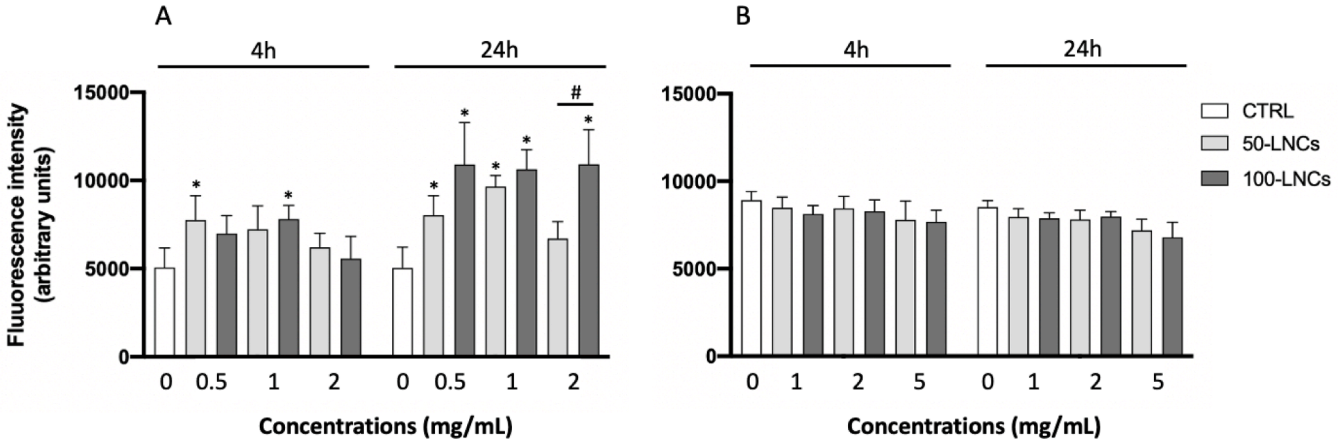

Fig. 8. Lipid peroxidation assessed on HepG2 (A) and HepaRG (B) cells after 4 and 24 h of exposure to 50- and 100-LNCs. Data are shown as fluorescence intensity (n = 3 or 4) ± SEM. * and # ($p < 0,05$) represent a significative difference compared to the respective control group and between LNCs size, respectively.

No significant difference (p-value = 0.1) was observed between both size of LNCs. Except after 24 h of exposure at 2 mg/mL, where no lipid peroxidation was induced by 50-LNCs compared to the control (and not for 100-LNCs). But, given that around 80 % of the HepG2 cells treated with the 50-LNCs were dead, it is difficult to exploit this result.

Lipid peroxidation was not detected in the HepaRG cells (Fig. 8. B).

4. Discussion

NPs, including LNCs, have a well-demonstrated hepatic tropism (Hoarau et al. 2004, Zhang et al. 2016, Resnier et al. 2019, Radwan et al. 2020, Ashour et al. 2021). Despite this liver accumulation, LNCs interactions with liver cells have not been studied sufficiently, particularly LNCs toxicity upon chronic exposure, even if these nanoparticles have been developed for chronic diseases such as cancers. For that purpose, the HepaRG cell line was selected as it is the closest cell line to primary hepatocytes that allows chronic exposure assessment. First, after 24 h of exposure to LNCs, above 80 % cell viability was observed for concentrations equal to or below than 0.5 mg/mL and 2 mg/mL of LNCs suspension in HepG2 and HepaRG cells, respectively. Thus, the low toxicity of the LNCs with hepatocytes was demonstrated below these concentrations. Similarly, LNCs showed a cell viability of approximately 80 % after 24 h of exposure to 50-LNCs at 2 mg/mL and 95 % with 100-LNCs at 3 mg/mL in an immortalized macrophage cell line (RAW264.7 cells) (Le Roux et al. 2017). Additionally, LNCs were significantly more toxic to HepG2 cells than to HepaRG cells. Indeed, the LC_{50} was multiplied 8 for 100-LNCs and by 4.5 for 50-LNCs in HepaRG cells (Table 3). Furthermore, LDH release was higher in HepG2 cells than that in HepaRG cells (Fig. 2). The difference in toxicity observed between the two hepatoma cell lines was confirmed by the NRU assay, which measured lysosomal activity (Supplementary data, Figure S1). HepaRG is the closest model to primary human hepatocytes (Andersson et al. 2012, Mueller et al. 2014), hence it can be extrapolated that LNCs would have limited side effects on hepatocytes, while potentializing the active drug's toxicity in hepatocarcinoma cells. For example, encapsulation of sorafenib (a drug widely used to treat HCC) into LNCs could have an interest in improving its activity for HCC treatment. Clavreul *et al.* already developed a sorafenib-loaded LNCs of 50 nm (Clavreul et al. 2018). In the present study, 50-LNCs at 1 mg/mL were considered safe regarding the toxicity in HepaRG cells, whereas for the same dose, the LC_{50} was reached in the HepG2 cell line. Therefore, LNCs could potentialize the efficacy of sorafenib on liver cancer cells while having minimal side effects on hepatocytes. This hypothesis should be explored with an *in vivo* experiment, comparing sorafenib loaded-LNCs *vs.* sorafenib alone after IV injection on HCC bearing models.

According to the literature, the size of NPs appears to influence their

toxicity: smaller NPs seem to induce greater toxicity. This tendance was observed on primary rat hepatocytes and HepaRG cells exposed to gold NPs (Enea et al. 2021), and also in liver after a unique IV injection of silver NPs in mice (Recordati et al. 2015). Moreover, in other cells, a similar behavior was displayed for LNCs on murine macrophages (Le Roux et al. 2017) and different glioma cell lines (Lamprecht et al., 2006). In this work, the toxicity assessment highlighted a statistically higher toxicity of 50-LNCs compared to 100-LNCs in both hepatoma cell lines. However, is toxicity only linked to the size of LNCs or is there another parameter, such as surfactant effect, to consider? Indeed, LNCs are formulated according to a solvent-free method that uses generally recommended as safe ("GRAS") excipients, and modifying their composition, notably the oily phase and non-ionic surfactant (Kolliphor® HS15), increases their size distribution (Heurtault et al. 2003). More precisely, the percentage of Kolliphor® was higher in the 50-LNCs than in the 100-LNCs (48 % *vs.* 33 % w/w as a function of all dry components, respectively). Le Roux *et al.* showed that smaller LNCs (25 and 50 nm) induced higher toxicity in a murine macrophage cell line, and Kolliphor® HS15 exhibited some toxicity by increasing nitric oxide production in RAW264.7 cells (Le Roux et al. 2017). Additionally, Maupas *et al.* showed that LNCs toxicity in HaCaT cells was correlated with the nature of the surfactant used (Maupas et al. 2011). They demonstrated that Kolliphor® HS15 was the second most toxic surfactant compared to others, followed by Cremophor® EL, Vitamin E TPGS®, Simulsol® 4000, polysorbate 20, and 80. Thus, LNCs toxicity could be linked to Kolliphor® HS15 and its amount is implicitly linked to the size of the particles, knowing that the smaller the size the higher the contact surface with cells.

Additionally, for the first time, chronic liver toxicity with repeated exposure to LNCs was studied to evaluate potential chronic liver side effects *in vitro*. Analysis of the LC_{50} showed that 50-LNCs induced time-dependent toxicity. The 100-LNCs were more toxic after 2 weeks of exposure *vs.* 24 h of exposure, but no more toxicity was observed after 2 supplementary weeks of treatment. In conclusion, 100-LNCs were less toxic to HepaRG cells, indicating that the side effects on liver parenchymal cells could be limited even after repeated exposure.

The kinetics of internalization is one of the most important parameters for the evaluation of nanoparticles because it affects their *in vitro* and *in vivo* behavior, and therefore, their use as therapeutics (Siegrist et al. 2019, Cornu et al. 2020). The 100- LNCs were internalized faster and accumulated more than the 50-LNCs after acute and chronic exposure in hepatocytes in liver cells. *In vivo* results from Hirsjärvi *et al.* showed a larger proportion of 100-LNCs accumulating inside the liver after 1.5 and 4 h of exposure, compared to 50-LNCs (Hirsjärvi et al. 2013). In the presence of proteins and other molecules contained in FBS, a protein corona around the NPs is expected to form (Tenzer et al. 2013, Lebreton et al. 2021). This protein corona play a crucial role in nanoparticle behavior by changing their physicochemical properties, thus becoming new nanoparticles and eventually altering their *in vitro/in vivo* fate (Lundqvist et al. 2008, Pareek et al. 2018). In a recent study, Lebreton *et al.* showed that the highest protein binding was obtained on 50-LNCs *vs.* 100-LNCs: it led to the formation of a thicker corona around the smaller LNCs (Lebreton et al. 2023). This thick corona can block binding sites and thus could explain our results. Furthermore, in the presence of FBS, internalization of LNCs in HepG2 cells was much lower: 5 *vs.* 85 % and 35 *vs.* 80 % after 30 min for 50- and 100-LNCs, respectively (Fig. 3 and Supplementary Data Figure S3). Similar results were obtained on HepaRG cells. Moreover, LNCs exhibited statistically less toxicity under 10 % FBS conditions compared to 0 % FBS conditions in HepG2 cells. Similar results were obtained with silica NPs in the HepG2 model (Choi et al. 2022). The authors demonstrated a drastic increase in LC_{50} and a decrease in the uptake velocity of NPs with FBS forming a protein corona. Ultimately, LNCs liver internalization and toxicity could depend on the size and formation of a protein corona, which should explain their behavior *in vivo*.

Then the pathways of internalization were studied. NPs in general are mainly dependent on endocytic mechanisms for entering the cells (Sousa De Almeida et al. 2021) and their size will condition the pathway they will go through. For NPs measuring around 200 nm or more, macropinocytosis and phagocytosis are the favored pathways to enter the cells (Gustafson et al. 2015, Claudia et al. 2017, Li and Pang 2021). Caveolin-mediated endocytosis (CavMe) and clathrin-mediated endocytosis (CME) form vesicles that can uptake NPs less than 200 nm (Brandenberger et al. 2010, Lammel et al. 2019, Mazumdar et al. 2021, Rennick et al. 2021, Means et al. 2022). In this study, LNCs were thus expected to be internalized via CavME or CME. First, an active internalization was confirmed using a 4 °C condition, which is known to be a general metabolic inhibitor also able to restrain pinocytic and endocytic uptake mechanisms (Tomoda et al. 1989, Verma et al. 2008). It is important to keep in mind that the fluidity of the cell membrane is also different at low temperature. Then, a major inhibition of LNCs internalization by genistein in both cells confirmed the involvement of CavMe without influence of size. In contrast, because chlorpromazine did not affect internalization, CME did not appear to be involved. Contrary to clathrin vesicles that will fuse with lysosomes and follow classic degradative endocytic pathway, a proportion a caveosomes is able to stay independent from this classic pathway and dodge lysosomal degradation. This would represent a real advantage for an active drug loaded into LNC that will escape lysosomal degradation (Kiss and Botos 2009). Furthermore, LNCs were still internalized via CavME after 4 weeks of exposure, which confirmed that repeated exposure did not affect the internalization pathways. In contrast, Paillard *et al.* showed that the size had influenced the pathways of internalization within malignant rat glioma cells (F98): 50-LNCs were internalized mainly via CME, whereas 100-LNCs were internalized via CME and CavME pathways (Paillard et al. 2010). Roger *et al.* also showed that paclitaxel-loaded LNCs were mainly transported across Caco-2 cell line (differentiated enterocytes) through endocytosis via CME, clathrin- and dynamin-independent endocytosis and CavME (Roger et al. 2009). It is important to note that disparities in LNCs internalization mechanisms are present between cell lines. Thus, it is difficult to predict which pathway will be taken for different nanoparticles on different cell lines.

To complete the semi-quantitative kinetic studies, a qualitative analysis of LNCs localization inside the intracellular compartment was performed using confocal microscopy. LNCs were visualized inside HepG2 cells after 1 h (data not shown) and were mostly localized in the cytoplasm after 2 h, with some colocalization with lysosomes for both LNCs sizes (Fig. 5). This result confirmed a quick uptake, which later probably fused with early and late endosomes and finally with lysosomes. Therefore, even if *endo*-lysosomal machinery was confirmed, it is already demonstrated that a proportion of LNCs might be escaping (Paillard et al. 2010).

Finally, the cell death mechanism(s) involved in LNCs internalization were studied. Although LNCs can trigger apoptosis in breast cancer cells, such as MCF-7 and B16F10 (Basu et al. 2021, Topin-Ruiz et al. 2021), no activation of apoptosis was detected at any concentration tested nor time of exposure in HepG2 and HepaRG cells (Fig. 6). Another type of cell death, ferroptosis, has been demonstrated using drugs and nanoparticles in some cell lines. For example, Yu *et al.* showed that erastin-loaded exosomes could induce ferroptosis in MDA-MB-231 cells by suppressing the expression of GPX4 (Yu et al. 2019). Moreover, oxidative stress and ferroptosis have been observed in breast cancer cells after exposure to LNCs (Szwed et al. 2020). FER, a specific ferroptosis inhibitor, binds to the 15LOX/PEBP1 complex, thereby decreasing lipid ROS (Anthonymuthu et al. 2021). In this work, the use of FER significantly increased the viability of HepG2 cells exposed to 50-LNCs only. For HepaRG cell line, FER could increase cell viability for both LNCs sizes (Fig. 7). Consequently, LNCs size may influence cell death mechanisms in HepG2 cells. Although cell viability increased with FER, values did not go back to 100 % for concentrations equal or upper to 1 mg/mL for HepG2 cells and 5 mg/mL for HepaRG cells. This result suggests that at high LNC concentrations, detoxification systems from

liver cells are overwhelmed and/or other death pathways are initiated, making it impossible for the cells to return to a normal physiological state. The release of LDH in both cellular models (reflecting membrane rupture) suggests that necrosis, parthanatos, necroptosis, or even oncosis may occur at these high concentrations and would be of interest to study (Galluzzi et al. 2018, Green 2019, Yan et al. 2020). Moreover, in the HepG2 cell line, lipid peroxidation was barely observable after 4 h of exposure but increased after 24 h. The cytotoxicity of LNCs could explain why lipid peroxidation was not observed for 50-LNCs after 24 h of exposure at a concentration of 2 mg/mL, as the LC_{50} was already reached and exceeded on HepG2 cells. In contrast, no lipid peroxidation was observed in HepaRG cells at any time of exposure. One hypothesis could be that cytotoxicity induced by LNCs below 5 mg/mL is too low to trigger lipid peroxidation. Unfortunately, no comparison is available in the literature as lipid peroxidation in HepaRG cells using Bodipy-C11 has not yet been studied. In the literature, only two studies have assessed lipid peroxidation in HepaRG using the quantification of malondialdehyde, but none of them was studying NPs (Do et al. 2013, Tobwala et al. 2015). So, this mechanism should be deeper explored.

5. Conclusion and perspectives

In conclusion, liver toxicity assessment highlighted a hood safety profile of LNCs at low and medium concentrations after acute and chronic exposure in the HepaRG cell line. Furthermore, 50-LNCs were more toxic than 100-LNCs despite slower internalization in both cell lines, and both LNCs mainly used an active mechanism of transport involving CavMe, regardless of size. Chronic exposure did not change LNCs internalization kinetics compared to acute 24 h exposure but their intracellular accumulation was raised although the pathways of internalization remained the same. The mechanism of toxicity involves lipid peroxidation and ferroptosis in cancerous HepG2 cells, and ferroptosis in differentiated HepaRG cells. Finally, 100-LNCs exhibited low toxicity in the HepaRG cell line after 4 weeks of exposure, without altering the kinetics nor pathways of internalization. This *in vitro* study provides a better understanding of the interactions between LNCs and hepatic cells and, for the first time, after repeated exposure over a month. Moreover, as it has been suggested with the presence of Kolliphor® HS15, composition may be a determining factor in toxicity. Thus, it could be interesting to vary the composition (different oils, hydrophilic or lipophilic surfactants, and their quantities) and study the impact on toxicity.

Finally, faster internalization associated with higher toxicity in hepatic cancer cells was demonstrated, opening a new perspective of using LNCs as nanomedicines to treat hepatocarcinoma. The preferential liver tumor distribution needs to be explored *in vivo* on HCC bearing models. In this context, the encapsulation of sorafenib, one of the first lines of treatment for advanced HCC (Blanc et al. 2021), into LNCs should be considered.

Funding

This work was supported by the Ligue Contre le Cancer, comité départemental du Maine et Loire (49) Committee (December 2020).

CRediT authorship contribution statement

Flavien Delaporte: . **Emilie Roger:** Writing – review & editing, Validation, Supervision, Resources, Project administration, Conceptualization. **Jérome Bejaud:** Investigation, Formal analysis. **Pascal Loyer:** Writing – review & editing, Visualization. **Frédéric Lagarce:** Writing – review & editing, Validation, Supervision. **Camille C. Savary:** Writing – review & editing, Visualization, Validation, Supervision, Resources, Project administration, Methodology, Funding acquisition, Formal analysis, Conceptualization.

Declaration of competing interest

The authors declare that they have no known competing financial interests or personal relationships that could have appeared to influence the work reported in this paper.

Data availability

The authors confirm that the data supporting the findings of this study are available in the article and/or its supplementary material.

Acknowledgements

We would like to thank Catherine Guillet from the PACEM platform (Angers) for her valuable help with the collection of the FACS data. With the same logic, we would like to thank Rodolphe Perrot, from SCIAM laboratory (Angers), for his help concerning the confocal microscopy acquisitions.

Appendix A. Supplementary material

Supplementary data to this article can be found online at https://doi.org/10.1016/j.ijpharm.2024.124815.

References

Ajdary, M., Moosavi, M., Rahmati, M., Falahati, M., Mahboubi, M., Mandegary, A., Jangjoo, S., Mohammadinejad, R., Varma, R., 2018. Health concerns of various nanoparticles: a review of their in vitro and in vivo toxicity. Nanomaterials 8 (9), 634.

Andersson, T.B., Kanebratt, K.P., Kenna, J.G., 2012. The HepaRG cell line: a unique *in vitro* tool for understanding drug metabolism and toxicology in human. Expert Opin. Drug Metab. Toxicol. 8 (7), 909–920.

Andrade, R.J., Chalasani, N., Björnsson, E.S., Suzuki, A., Kullak-Ublick, G.A., Watkins, P. B., Devarbhavi, H., Merz, M., Lucena, M.I., Kaplowitz, N., Aithal, G.P., 2019. Drug-induced liver injury. Nat. Rev. Dis. Primers 5 (1), 58.

Anthérieu, S., Chesné, C., Li, R., Camus, S., Lahoz, A., Picazo, L., Turpeinen, M., Tolonen, A., Uusitalo, J., Guguen-Guillouzo, C., Guillouzo, A., 2010. Stable expression, activity, and inducibility of cytochromes P450 in differentiated HepaRG cells. Drug Metab. Dispos. 38 (3), 516–525.

Anthonymuthu, T.S., Tyurina, Y.Y., Sun, W.-Y., Mikulska-Ruminska, K., Shrivastava, I.H., Tyurin, V.A., Cinemre, F.B., Dar, H.H., VanDemark, A.P., Holman, T.R., Sadovsky, Y., Stockwell, B.R., He, R.-R., Bahar, I., Bayır, H., Kagan, V.E., 2021. Resolving the paradox of ferroptotic cell death: Ferrostatin-1 binds to 15LOX/PEBP1 complex, suppresses generation of peroxidized ETE-PE, and protects against ferroptosis. Redox Biol. 38, 101744.

Ashour, A.A., El-Kamel, A.H., Abdelmonsif, D.A., Khalifa, H.M., Ramadan, A.A., 2021. Modified lipid nanocapsules for targeted tanshinone IIA delivery in liver fibrosis. Int. J. Nanomed. 16, 8013–8033.

Barenholz (Chezy), Y., 2012. Doxil® — the first FDA-approved nano-drug: Lessons learned. J. Control. Release 160 (2), 117–134.

Basile, L., Pignatello, R., Passirani, C., 2012. Active targeting strategies for anticancer drug nanocarriers. Curr. Drug Deliv. 9 (3), 255–268.

Basu, S.M., Yadava, S.K., Singh, R., Giri, J., 2021. Lipid nanocapsules co-encapsulating paclitaxel and salinomycin for eradicating breast cancer and cancer stem cells. Colloids Surf. B Biointerf. 204, 111775.

Bian, Q., Liu, J., Tian, J., Hu, Z., 2004. Binding of genistein to human serum albumin demonstrated using tryptophan fluorescence quenching. Int. J. Biol. Macromol. 34 (5), 275–279.

Blanc, J.F., Debaillon-Vesque, A., Roth, G., Barbare, J.C., Baumann, A.S., Boige, V., Boudjema, K., Bouattour, M., Crehange, G., Dauvois, B., Decaens, T., Dewaele, F., Farges, O., Guiu, B., Hollebecque, A., Merle, P., Selves, J., Aparicio, T., Ruiz, I., Bouché, O., 2021. Hepatocellular carcinoma: french intergroup clinical practice guidelines for diagnosis, treatment and follow-up (SNFGE, FFCD, GERCOR, UNICANCER, SFCD, SFED, SFRO, AFEF, SIAD, SFR/FRI). Clin. Res. Hepatol. Gastroenterol. 45 (2), 101590.

Brandenberger, C., Mühlfeld, C., Ali, Z., Lenz, A.-G., Schmid, O., Parak, W.J., Gehr, P., Rothen-Rutishauser, B., 2010. Quantitative evaluation of cellular uptake and trafficking of plain and polyethylene glycol-coated gold nanoparticles. Small 6 (15), 1669–1678.

Cerec, V., Glaise, D., Garnier, D., Morosan, S., Turlin, B., Drenou, B., Gripon, P., Kremsdorf, D., Guguen-Guillouzo, C., Corlu, A., 2007. Transdifferentiation of hepatocyte-like cells from the human hepatoma HepaRG cell line through bipotent progenitor. Hepatology 45 (4), 957–967.

Choi, J.W., Kim, I.Y., Kwak, M., Kim, J., Yoon, S., Jang, H.J., Lee, T.G., Heo, M.B., 2022. Effect of serum protein on cell internalization of silica nanoparticles. Micro & Nano Lett. 17 (3), 59–67.

Claudia, M., Kristin, Ö., Jennifer, O., Eva, R., Eleonore, F., 2017. Comparison of fluorescence-based methods to determine nanoparticle uptake by phagocytes and non-phagocytic cells in vitro. Toxicology 378, 25–36.
Clavreul, A., Roger, E., Pourbaghi-Masouleh, M., Lemaire, L., Tétaud, C., Menei, P., 2018. Development and characterization of sorafenib-loaded lipid nanocapsules for the treatment of glioblastoma. Drug Deliv. 25 (1), 1756–1765.
Cornu, R., Béduneau, A., Martin, H., 2020. Influence of nanoparticles on liver tissue and hepatic functions: a review. Toxicology 430, 152344.
Dabholkar, N., Waghule, T., Krishna Rapalli, V., Gorantla, S., Alexander, A., Narayan Saha, R., Singhvi, G., 2021. Lipid shell lipid nanocapsules as smart generation lipid nanocarriers. J. Mol. Liq. 339, 117145.
Desai, P.P., Date, A.A., Patravale, V.B., 2012. Overcoming poor oral bioavailability using nanoparticle formulations – opportunities and limitations. Drug Discov. Today Technol. 9 (2), e87–e95.
Do, T.H.T., Gaboriau, F., Cannie, I., Batusanski, F., Ropert, M., Moirand, R., Brissot, P., Loreal, O., Lescoat, G., 2013. Iron-mediated effect of alcohol on hepatocyte differentiation in HepaRG cells. Chem. Biol. Interact. 206 (2), 117–125.
Enea, M., Pereira, E., Costa, J., Soares, M.E., Dias da Silva, D., de Bastos, M.L., Carmo, H. F., 2021. Cellular uptake and toxicity of gold nanoparticles on two distinct hepatic cell models. Toxicol. In Vitro 70, 105046.
Fadeel, B., Fornara, A., Toprak, M.S., Bhattacharya, K., 2015. Keeping it real: the importance of material characterization in nanotoxicology. Biochem. Biophys. Res. Commun. 468 (3), 498–503.
Frank, L.A., Contri, R.V., Beck, R.C.R., Pohlmann, A.R., Guterres, S.S., 2015. Improving drug biological effects by encapsulation into polymeric nanocapsules: Improving drug effects by nanocapsules. Wiley Interdiscip. Rev. Nanomed. Nanobiotechnol. 7 (5), 623–639.
Galluzzi, L., Vitale, I., Aaronson, S.A., Abrams, J.M., Adam, D., Agostinis, P., Alnemri, E. S., Altucci, L., Amelio, I., Andrews, D.W., Annicchiarico-Petruzzelli, M., Antonov, A. V., Arama, E., Baehrecke, E.H., Barlev, N.A., Bazan, N.G., Bernassola, F., Bertrand, M.J.M., Bianchi, K., Blagosklonny, M.V., Blomgren, K., Borner, C., Boya, P., Brenner, C., Campanella, M., Candi, E., Carmona-Gutierrez, D., Cecconi, F., Chan, F.-K.-M., Chandel, N.S., Cheng, E.H., Chipuk, J.E., Cidlowski, J.A., Ciechanover, A., Cohen, G.M., Conrad, M., Cubillos-Ruiz, J.R., Czabotar, P.E., D'Angiolella, V., Dawson, T.M., Dawson, V.L., De Laurenzi, V., De Maria, R., Debatin, K.-M., DeBerardinis, R.J., Deshmukh, M., Di Daniele, N., Di Virgilio, F., Dixit, V.M., Dixon, S.J., Duckett, C.S., Dynlacht, B.D., El-Deiry, W.S., Elrod, J.W., Fimia, G.M., Fulda, S., García-Sáez, A.J., Garg, A.D., Garrido, C., Gavathiotis, E., Golstein, P., Gottlieb, E., Green, D.R., Greene, L.A., Gronemeyer, H., Gross, A., Hajnoczky, G., Hardwick, J.M., Harris, I.S., Hengartner, M.O., Hetz, C., Ichijo, H., Jäättelä, M., Joseph, B., Jost, P.J., Juin, P.P., Kaiser, W.J., Karin, M., Kaufmann, T., Kepp, O., Kimchi, A., Kitsis, R.N., Klionsky, D.J., Knight, R.A., Kumar, S., Lee, S.W., Lemasters, J.J., Levine, B., Linkermann, A., Lipton, S.A., Lockshin, R.A., López-Otín, C., Lowe, S.W., Luedde, T., Lugli, E., MacFarlane, M., Madeo, F., Malewicz, M., Malorni, W., Manic, G., Marine, J.-C., Martin, S.J., Martinou, J.-C., Medema, J.P., Mehlen, P., Meier, P., Melino, S., Miao, E.A., Molkentin, J.D., Moll, U.M., Muñoz-Pinedo, C., Nagata, S., Nuñez, G., Oberst, A., Oren, M., Overholtzer, M., Pagano, M., Panaretakis, T., Pasparakis, M., Penninger, J.M., Pereira, D.M., Pervaiz, S., Peter, M. E., Piacentini, M., Pinton, P., Prehn, J.H.M., Puthalakath, H., Rabinovich, G.A., Rehm, M., Rizzuto, R., Rodrigues, C.M.P., Rubinsztein, D.C., Rudel, T., Ryan, K.M., Sayan, E., Scorrano, L., Shao, F., Shi, Y., Silke, J., Simon, H.-U., Sistigu, A., Stockwell, B.R., Strasser, A., Szabadkai, G., Tait, S.W.G., Tang, D., Tavernarakis, N., Thorburn, A., Tsujimoto, Y., Turk, B., Vanden Berghe, T., Vandenabeele, P., Vander Heiden, M.G., Villunger, A., Virgin, H.W., Vousden, K.H., Vucic, D., Wagner, E.F., Walczak, H., Wallach, D., Wang, Y., Wells, J.A., Wood, W., Yuan, J., Zakeri, Z., Zhivotovsky, B., Zitvogel, L., Melino, G., Kroemer, G., 2018. Molecular mechanisms of cell death: recommendations of the Nomenclature Committee on Cell Death 2018. Cell Death Differ. 25 (3), 486–541.
Green, D.R., 2019. The coming decade of cell death research: five riddles. Cell 177 (5), 1094–1107.
Gustafson, H.H., Holt-Casper, D., Grainger, D.W., Ghandehari, H., 2015. Nanoparticle uptake: the phagocyte problem. Nano Today 10 (4), 487–510.
Heurtault, B., Saulnier, P., Pech, B., Proust, J.-E., and Benoit, J.-P., 2002. A Novel Phase Inversion-Based Process for the Preparation of Lipid Nanocarriers, 6.
Heurtault, B., Saulnier, P., Pech, B., Venier-Julienne, M.-C., Proust, J.-E., Phan-Tan-Luu, R., Benoît, J.-P., 2003. The influence of lipid nanocapsule composition on their size distribution. Eur. J. Pharm. Sci. 18 (1), 55–61.
Hirsjärvi, S., Dufort, S., Gravier, J., Texier, I., Yan, Q., Bibette, J., Sancey, L., Josserand, V., Passirani, C., Benoit, J.-P., Coll, J.-L., 2013. Influence of size, surface coating and fine chemical composition on the in vitro reactivity and in vivo biodistribution of lipid nanocapsules versus lipid nanoemulsions in cancer models. Nanomed. Nanotechnol. Biol. Med. 9 (3), 375–387.
Hoarau, D., Delmas, P., David, S., Roux, E., Leroux, J.-C., 2004. Novel long-circulating lipid nanocapsules. Pharm. Res. 21 (10), 1783–1789.
Hureaux, J., Lagarce, F., Gagnadoux, F., Rousselet, M.-C., Moal, V., Urban, T., Benoit, J.-P., 2010. Toxicological study and efficacy of blank and paclitaxel-loaded lipid nanocapsules after i.v. administration in mice. Pharm. Res. 27 (3), 421–430.
Huynh, N.T., Passirani, C., Saulnier, P., Benoit, J.P., 2009. Lipid nanocapsules: a new platform for nanomedicine. Int. J. Pharm. 379 (2), 201–209.
Jossé, R., Aninat, C., Glaise, D., Dumont, J., Fessard, V., Morel, F., Poul, J.-M., Guguen-Guillouzo, C., Guillouzo, A., 2008. Long-term functional stability of human heparg hepatocytes and use for chronic toxicity and genotoxicity studies. Drug Metab. Dispos. 36 (6), 1111–1118.
Kammerer, S., Küpper, J.-H., 2018. Human hepatocyte systems for in vitro toxicology analysis. J. Cell. Biotechnol. 3 (2), 85–93.
Kilin, V.N., Anton, H., Anton, N., Steed, E., Vermot, J., Vandamme, T.F., Mely, Y., Klymchenko, A.S., 2014. Counterion-enhanced cyanine dye loading into lipid nano-droplets for single-particle tracking in zebrafish. Biomaterials 35 (18), 4950–4957.
Kiss, A.L., Botos, E., 2009. Endocytosis *via* caveolae: alternative pathway with distinct cellular compartments to avoid lysosomal degradation? J. Cell Mol. Med. 13 (7), 1228–1237.
Lammel, T., Mackevica, A., Johansson, B.R., Sturve, J., 2019. Endocytosis, intracellular fate, accumulation, and agglomeration of titanium dioxide (TiO2) nanoparticles in the rainbow trout liver cell line RTL-W1. Environ. Sci. Pollut. Res. 26 (15), 15354–15372.
Lamprecht, A., Benoit, J.-P., 2006. Etoposide nanocarriers suppress glioma cell growth by intracellular drug delivery and simultaneous P-glycoprotein inhibition. J. Control. Release 112 (2), 208–213.
Le Roux, G., Moche, H., Nieto, A., Benoit, J.-P., Nesslany, F., Lagarce, F., 2017. Cytotoxicity and genotoxicity of lipid nanocapsules. Toxicol. In Vitro 41, 189–199.
Lebreton, V., Legeay, S., Saulnier, P., Lagarce, F., 2021. Specificity of pharmacokinetic modeling of nanomedicines. Drug Discov. Today 26 (10), 2259–2268.
Lebreton, V., Legeay, S., Vasylaki, A., Lagarce, F., Saulnier, P., 2023. Protein corona formation on lipidic nanocapsules: Influence of the interfacial PEG repartition. Eur. J. Pharm. Sci. 189, 106537.
Li, Y.-X., Pang, H.-B., 2021. Macropinocytosis as a cell entry route for peptide-functionalized and bystander nanoparticles. J. Control. Release 329, 1222–1230.
Lundqvist, M., Stigler, J., Elia, G., Lynch, I., Cedervall, T., Dawson, K.A., 2008. Nanoparticle size and surface properties determine the protein corona with possible implications for biological impacts. Proc. Natl. Acad. Sci. 105 (38), 14265–14270.
Marshak, D.R., Lukas, T.J., Watterson, D.M., 1985. Drug-protein interactions: binding of chlorpromazine to calmodulin, calmodulin fragments, and related calcium binding proteins. Biochemistry 24 (1), 144–150.
Maupas, C., Moulari, B., Béduneau, A., Lamprecht, A., Pellequer, Y., 2011. Surfactant dependent toxicity of lipid nanocapsules in HaCaT cells. Int. J. Pharm. 411 (1–2), 136–141.
Mazumdar, S., Chitkara, D., Mittal, A., 2021. Exploration and insights into the cellular internalization and intracellular fate of amphiphilic polymeric nanocarriers. Acta Pharm. Sin. B 11 (4), 903–924.
Means, N., Elechalawar, C.K., Chen, W.R., Bhattacharya, R., Mukherjee, P., 2022. Revealing macropinocytosis using nanoparticles. Mol. Aspects Med. 83, 100993.
Montigaud, Y., Ucakar, B., Krishnamachary, B., Bhujwalla, Z.M., Feron, O., Préat, V., Danhier, F., Gallez, B., Danhier, P., 2018. Optimized acriflavine-loaded lipid nanocapsules as a safe and effective delivery system to treat breast cancer. Int. J. Pharm. 551 (1–2), 322–328.
Mouzouvi, C.R.A., Umerska, A., Bigot, A.K., Saulnier, P., 2017. Surface active properties of lipid nanocapsules. PLoS One 12 (8), e0179211.
Mueller, D., Krämer, L., Hoffmann, E., Klein, S., Noor, F., 2014. 3D organotypic HepaRG cultures as in vitro model for acute and repeated dose toxicity studies. Toxicol. In Vitro 28 (1), 104–112.
Paillard, A., Hindré, F., Vignes-Colombeix, C., Benoit, J.-P., Garcion, E., 2010. The importance of endo-lysosomal escape with lipid nanocapsules for drug subcellular bioavailability. Biomaterials 31 (29), 7542–7554.
Pareek, V., Bhargava, A., Bhanot, V., Gupta, R., Jain, N., Panwar, J., 2018. Formation and Characterization of Protein Corona Around Nanoparticles: A Review. J. Nanosci. Nanotechnol. 18 (10), 6653–6670.
Protocols - Nanotechnology Characterization Lab - NCI [online], 2022. Available from: https://www.cancer.gov/nano/research/ncl/protocols-capabilities [Accessed 24 May 2023].
Radwan, S.A.A., El-Maadawy, W.H., ElMeshad, A.N., Shoukri, R.A., Yousry, C., 2020. Impact of reverse micelle loaded lipid nanocapsules on the delivery of gallic acid into activated hepatic stellate cells: a promising therapeutic approach for hepatic fibrosis. Pharm. Res. 37 (9), 180.
Recordati, C., De Maglie, M., Bianchessi, S., Argentiere, S., Cella, C., Mattiello, S., Cubadda, F., Aureli, F., D'Amato, M., Raggi, A., Lenardi, C., Milani, P., Scanziani, E., 2015. Tissue distribution and acute toxicity of silver after single intravenous administration in mice: nano-specific and size-dependent effects. Part. Fibre Toxicol. 13 (1), 12.
Rennick, J.J., Johnston, A.P.R., Parton, R.G., 2021. Key principles and methods for studying the endocytosis of biological and nanoparticle therapeutics. Nat. Nanotechnol. 16 (3), 266–276.
Resnier, P., Lepeltier, E., Emina, A.L., Galopin, N., Bejaud, J., David, S., Ballet, C., Benvegnu, T., Pecorari, F., Chourpa, I., Benoit, J.-P., Passirani, C., 2019. Model Affitin and PEG modifications onto siRNA lipid nanocapsules: cell uptake and *in vivo* biodistribution improvements. RSC Adv. 9 (47), 27264–27278.
Roger, E., Lagarce, F., Garcion, E., Benoit, J.-P., 2009. Lipid nanocarriers improve paclitaxel transport throughout human intestinal epithelial cells by using vesicle-mediated transcytosis. J. Control. Release 140 (2), 174–181.
Roger, E., Gimel, J.-C., Bensley, C., Klymchenko, A.S., Benoit, J.-P., 2017. Lipid nanocapsules maintain full integrity after crossing a human intestinal epithelium model. J. Control. Release 253, 11–18.
Schaffazick, S.R., Siqueira, I.R., Badejo, A.S., Jornada, D.S., Pohlmann, A.R., Netto, C.A., Guterres, S.S., 2008. Incorporation in polymeric nanocapsules improves the antioxidant effect of melatonin against lipid peroxidation in mice brain and liver. Eur. J. Pharm. Biopharm. 69 (1), 64–71.
Siegrist, S., Cörek, E., Detampel, P., Sandström, J., Wick, P., Huwyler, J., 2019. Preclinical hazard evaluation strategy for nanomedicines. Nanotoxicology 13 (1), 73–99.
Sousa De Almeida, M., Susnik, E., Drasler, B., Taladriz-Blanco, P., Petri-Fink, A., Rothen-Rutishauser, B., 2021. Understanding nanoparticle endocytosis to improve targeting strategies in nanomedicine. Chem. Soc. Rev. 50 (9), 5397–5434.

Szwed, M., Torgersen, M.L., Kumari, R.V., Yadava, S.K., Pust, S., Iversen, T.G., Skotland, T., Giri, J., Sandvig, K., 2020. Biological response and cytotoxicity induced by lipid nanocapsules. J. Nanobiotechnol. 18 (1), 5.
Tenzer, S., Docter, D., Kuharev, J., Musyanovych, A., Fetz, V., Hecht, R., Schlenk, F., Fischer, D., Kiouptsi, K., Reinhardt, C., Landfester, K., Schild, H., Maskos, M., Knauer, S.K., Stauber, R.H., 2013. Rapid formation of plasma protein corona critically affects nanoparticle pathophysiology. Nat. Nanotechnol. 8 (10), 772–781.
Tobwala, S., Khayyat, A., Fan, W., Ercal, N., 2015. Comparative evaluation of N-acetylcysteine and N-acetylcysteineamide in acetaminophen-induced hepatotoxicity in human hepatoma HepaRG cells. Exp. Biol. Med. 240 (2), 261–272.
Tomoda, H., Kishimoto, Y., Lee, Y.C., 1989. Temperature effect on endocytosis and exocytosis by rabbit alveolar macrophages. J. Biol. Chem. 264 (26), 15445–15450.
Topin-Ruiz, S., Mellinger, A., Lepeltier, E., Bourreau, C., Fouillet, J., Riou, J., Jaouen, G., Martin, L., Passirani, C., Clere, N., 2021. p722 ferrocifen loaded lipid nanocapsules improve survival of murine xenografted-melanoma via a potentiation of apoptosis and an activation of CD8+ T lymphocytes. Int. J. Pharm. 593, 120111.
Verma, A., Uzun, O., Hu, Y., Hu, Y., Han, H.-S., Watson, N., Chen, S., Irvine, D.J., Stellacci, F., 2008. Surface-structure-regulated cell-membrane penetration by monolayer-protected nanoparticles. Nat. Mater. 7 (7), 588–595.
Yan, G., Elbadawi, M., Efferth, T., 2020. Multiple cell death modalities and their key features (Review). World Acad. Sci. J.
Yu, M., Gai, C., Li, Z., Ding, D., Zheng, J., Zhang, W., Lv, S., Li, W., 2019. Targeted exosome-encapsulated erastin induced ferroptosis in triple negative breast cancer cells. Cancer Sci. 110 (10), 3173–3182.
Zhang, Y.-N., Poon, W., Tavares, A.J., McGilvray, I.D., Chan, W.C.W., 2016. Nanoparticle–liver interactions: cellular uptake and hepatobiliary elimination. J. Control. Release 240, 332–348.